

Relationship Between Atmospheric Rivers and the Dry Season Extreme Precipitation in Central-Western Mexico

H. A. Inda-Díaz¹, T. A. O'Brien^{2,1}

¹Climate and Ecosystem Sciences Division, Lawrence Berkeley National Laboratory, Berkeley, CA, USA

²Dept. of Earth and Atmospheric Sciences, Indiana University, Bloomington, IN, USA

Key Points:

- Extreme precipitation during the dry season in Central-Western Mexico is associated with atmospheric rivers (ARs)
- The meteorological state during extreme precipitation events shows ideal conditions for orographic precipitation over the Sierra Madre
- A detector designed for tropical latitudes could increase the correlation between ARs and dry season precipitation over Central-Western Mexico

Abstract

Atmospheric rivers (AR) are long, narrow jets of moisture transport responsible for over 90% of the extreme precipitation in central-western Mexico (CWM) during the dry seasons (November-March) in the 1900-2010 period. We find that more than 25% of extreme precipitation amount and frequency are associated with ARs, with a maximum of 60%-80% during December and January near the coast of Sinaloa (107.5W, 25N). Composites of the mean meteorological state show "ideal" conditions for orographic precipitation due to landfalling ARs: high horizontal vapor transport perpendicular to the Sierra Madre. We observe a tropospheric wave pattern in vertical velocity, surface pressure, and geopotential height associated with these events. The nature and evolution of these waves need to be further studied. Our results suggest that TECA-BARD provides a reasonable estimation for AR presence in CWM. Nevertheless, we recommend using multiple AR detectors and one tuned explicitly for tropical latitudes. This will allow investigation of the response of CWM landfalling ARs and the region's hydroclimatology under future climate scenarios.

Plain Language Summary

Atmospheric rivers (ARs) are a meteorological phenomenon with strong poleward water vapor transport. Due to their important role in the hydrological cycle and water availability of midlatitudes (like California, Europe, and Chile, among others) and polar regions, the scientific community has mainly focused AR research on these regions. It was not until recently that AR in lower tropical latitudes gathered more attention. This work focuses on the relationship between ARs and the dry season (November-March) precipitation over Central-Western Mexico (CWM), around 25 degrees north over the Pacific Coast of Mexico. We use precipitation data from the ERA-20C reanalysis, observational dataset, and a Bayesian AR detector to show that most of the precipitation over CWM during the November-March season is due to meteorological features with similar characteristics to midlatitude ARs. These events show typical conditions for ARs orographic precipitation: high water vapor transport perpendicular to the Sierra Madre that condenses into rain when the mountains lift it. We believe that an AR detector specifically designed for tropical latitudes could increase the relationship between AR and November-March precipitation in CWM and better allow us to study how these events might be modified by climate change.

1 Introduction

Atmospheric rivers (AR) are long, narrow jets of moisture transport typically associated with a low-level jet stream ahead of the cold front of an extratropical cyclone (F. M. Ralph et al., 2018). ARs account for over 90% of the water vapor transport from the subtropics to midlatitudes (Zhu & Newell, 1998). Over the last 20 years, there has been an increasing interest in the study and characterization of ARs. Numerous recent studies investigate AR and their relationship with extreme wind, precipitation, their impact on the regional hydrological cycles, water mass balance, and extreme hydrological events like flooding and droughts in midlatitude continental regions like North America, Europe, and South America (Neiman et al., 2002; F. M. Ralph et al., 2004, 2005, 2006; Dirmeyer & Brubaker, 2007; Neiman et al., 2008; Leung & Qian, 2009; Guan et al., 2010; Viale & Nuñez, 2011; M. Dettinger, 2011; F. M. Ralph & Dettinger, 2011; Warner et al., 2012; M. D. Dettinger, 2013; Lavers & Villarini, 2013b, 2013a; Kim et al., 2013; Neiman et al., 2013; F. M. Ralph et al., 2013; Rutz et al., 2014; Gimeno et al., 2016; Lavers, Waliser, et al., 2016; Lavers, Pappenberger, et al., 2016; Waliser & Guan, 2017; Gershunov et al., 2017; Goldenson et al., 2018; Viale et al., 2018; Eldardiry et al., 2019; F. M. Ralph et al., 2019; Huang et al., 2021). Some works have even investigated the structure of AR

64 using *in situ* data and satellite observations (F. M. Ralph et al., 2005; Neiman et al., 2008;
65 F. M. Ralph et al., 2010).

66 The significant impact of ARs on the climatology and hydrology of midlatitudes
67 has generated great interest and community effort in studying ARs and their impacts
68 on these regions. (F. Ralph et al., 2019) introduced a scale to categorize AR strength
69 based on vapor transport intensity and landfall duration and show that there are ben-
70 efiticial and hazardous impacts associated with AR events. This scale is helpful for the
71 scientific community, and it is a way of communication with the general public. The AR
72 category scale can be applied to gridded datasets such as reanalysis, forecast, and cli-
73 mate projections. There is also an increasing interest in understanding how ARs and their
74 impact will change in future climates. (Payne et al., 2020) concludes that AR response
75 to climate change will have noticeable importance to water balance and regional water
76 resources.

77 Most of the ARs research focuses on midlatitudes and polar regions. ARs in low
78 latitudes are starting to generate interest within the scientific AR community. This work
79 is motivated by the lack of study of tropical ARs. Moreover, we are also motivated by
80 the direct observation of “unusual non-tropical” precipitation in the Winter of 2019-2020
81 in Nayarit, Mexico $\sim 21.5^{\circ}\text{N}, 104.9^{\circ}\text{W}$, during the dry season (November-March). We re-
82 fer to “unusual non-tropical” precipitation as a low magnitude precipitation rate (com-
83 pared to convective heavy tropical precipitation). During these days, we observed con-
84 stant rainfall throughout one or two days, very similar to typical California winter pre-
85 cipitation (Figure 1(b) shows the IVT and horizontal wind speed at 700 hPa from one
86 such event). The similarities in the IVT field with the typical characteristics of an AR
87 raised the question: *is this an AR? Are there more events like this, and how are they as-
88 sociated with the extreme precipitation for the dry season in Central-Western Mexico (CWM)?*
89 (thick black contour in Figure 1(a)).

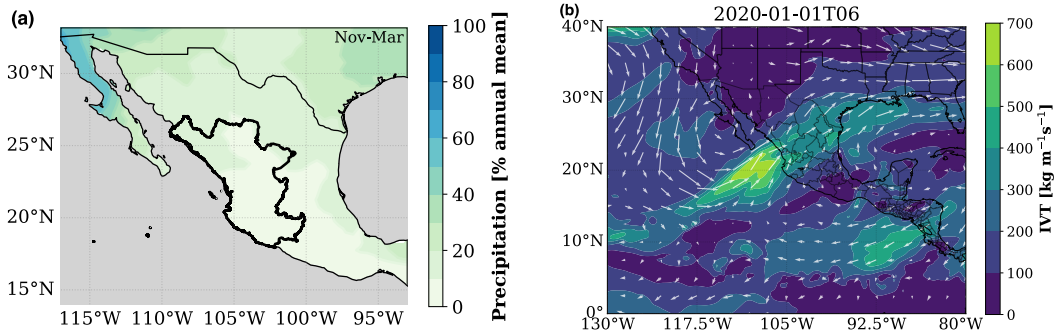


Figure 1. (a) Percentage of annual total precipitation from CPC Global Unified Gauge-Based Analysis of Daily Precipitation. Thick black contour is used to indicate what is considered as Central-Western Mexico throughout this work. (b) ERA5 reanalysis IVT in color contours. Vectors represent the 750 hPa wind velocity. 2020-01-01 is one of the times when the precipitation in CWM resembled the winter Californian AR-associated rainfall.

90 CWM is characterized by a dry season from November to March (García Amaro de
91 Miranda, 2003), with a mean monthly accumulated precipitation of less than 10 mm^1
92 and over 75% of the annual precipitation from July-September, during the spring and

¹ <https://smn.conagua.gob.mx/es/climatologia/temperaturas-y-lluvias/resumenes-mensuales-de-temperaturas-y-lluvias>

93 summer months. Rainfall in CWM is mainly associated with the North American Mon-
 94soon. Less than 10% of the total annual mean rainfall occurs between November and March
 95 for most of CWM (Figure 1(a)), according to the CPC Global Unified Gauge-Based Anal-
 96ysis of Daily Precipitation² (Chen et al., 2008).

97 From a socio-economic point of view, it is important to study and quantify these
 98 events of atypical precipitation. CWM is one of the largest agricultural production re-
 99 gions in Mexico. It is common knowledge among CWM farmers that these rainfall events
 100 can be exploited to benefit agriculture; however, we could not find scientific quantifica-
 101 tion of it. There are even popular beliefs that they can be predicted following a set of
 102 heuristic rules (Cruz López, 2011). There is also some evidence that different crops, like
 103 beans, coffee, and corn, are sensitive to changes in environmental conditions, like pre-
 104 cipitation and humidity (Viguera et al., 2017). Therefore, changes in climate conditions
 105 can affect the productivity and quality of the crops (Porter & Semenov, 2005).

106 Moreover, changes in wind speed and direction, moisture transport, and the loca-
 107 tion of the intertropical convergence zone (ITCZ) can modify the energy exchange be-
 108 tween the atmosphere and the ocean. These changes could generate a displacement north-
 109 ward of the oxygen minimum zone (OMZ), which can affect ocean species distribution
 110 and the productivity of regional aquaculture and fisheries (Breitburg, Denise; Grégoire,
 111 Marilaure and Isensee, Kirsten, 2018). Furthermore, other studies have observed that
 112 dry season rainfall events can change the coastal environment. Coastal water chlorophyll
 113 concentration, turbidity, temperature, and salinity, due to increased river discharge, can
 114 impact the sustainability of coastal ecosystems and their biological production (Domínguez-
 115 Hernández et al., 2020; Romero-Rodríguez et al., 2020).

116 Although there are numerous possible effects of anomalous winter precipitation in
 117 the CWM region, there is still a lack of documentation about these events and their im-
 118 pacts. Moreover, no existing research links these events with ARs. We investigate the
 119 relationship between lower latitudes ARs “dry season” (November–March) rainfall in CWM.
 120 We use data from the European Centre for Medium-Range Weather Forecasts (ECMWF)
 121 Atmospheric Reanalysis of the Twentieth Century ERA-20C³ (Poli et al., 2016) and the
 122 Bayesian AR Detector TECA-BARD v1.0.1. We aim to quantify how much of the CWM
 123 winter precipitation is associated with ARs and the meteorological state of the atmo-
 124 sphere during these events.

125 2 Data and Methods

126 ERA-20C output is 3-hourly with a of ~125 km on 37 pressure levels. We use data
 127 at pressure level: geopotential z , wind velocity u , v , and w , specific humidity q , temper-
 128 ature t , and surface level: mean sea level pressure mslp , surface pressure ps , total pre-
 129 precipitation tp , vertical integral of northward water vapor flux vinwvf , vertical integral
 130 of eastward water vapor flux viewvf , and total column water vapor tcwv . According to
 131 the ERA-20C documentation, the vertically integrated vapor fluxes are calculated in the
 132 model coordinates following:

$$\text{VIEWVF} = -\frac{1}{g} \int_0^1 qu \frac{\partial p}{\partial \eta} d\eta \approx -\frac{1}{g} \sum_{k=1}^N u_k q_k \Delta p_k, \quad (1)$$

$$\text{VINWVF} = -\frac{1}{g} \int_0^1 qv \frac{\partial p}{\partial \eta} d\eta \approx -\frac{1}{g} \sum_{k=1}^N v_k q_k \Delta p_k, \quad (2)$$

² <https://psl.noaa.gov/data/gridded/data.cpc.globalprecip.html>

³ <https://www.ecmwf.int/en/forecasts/datasets/reanalysis-datasets/era-20c>

133 where u and v are the components of the horizontal wind vector, q is the specific humidity,
 134 p is pressure, η is the hybrid coordinate (Simmons & Burridge, 1981), index k corresponds
 135 to model levels going from the surface ($k = 1$) to the top of the model atmosphere
 136 ($k = N$), and Δp_k is the difference in level pressures, estimated at level k . ERA-
 137 20C daily forecasted precipitation accumulation has been converted to a 3-hourly pre-
 138 cipitation rate (with units of mm/d); IWV is used directly from ERA-20C total column
 139 water vapor tcwv . IVT is calculated as the magnitude of the vertically integrated moisture-
 140 weighted wind (horizontal vapor flux vector) \vec{u}_q , directly from ERA-20C eastward and
 141 northward water vapor fluxes:

$$\vec{u}_q = (\text{VIEWVF}, \text{VINWVF}), \quad (3)$$

$$\text{IVT} = |\vec{u}_q| = \sqrt{\text{VIEWVF}^2 + \text{VINWVF}^2}. \quad (4)$$

142 Additionally, we compare the ERA-20C reanalysis data with observational precipitation,
 143 using precipitation data from the Livneh gridded precipitation for the continental US,
 144 Mexico, and Southern Canada (Livneh, Ben & National Center for Atmospheric
 145 Research Staff (Eds), Last modified 12 Dec 2019). The (Livneh et al., 2015) dataset is
 146 a long-term gridded daily dataset at fine $1/16^\circ$ (~ 6 km) horizontal resolution for the pe-
 147 riod 1950-2013. We use bilinear interpolation to regrid the AR detection from TECA-
 148 BARD in ERA-20C data to the Livneh dataset grid.

149 2.1 AR probability from ERA-20C and TECA-BARD

150 To calculate the probability of the presence of an atmospheric river (AR probability)
 151 we use the Bayesian AR Detector TECA-BARD v1.0.1, a probabilistic AR detector
 152 implemented in the Toolkit for Extreme Climate Analysis TECA. TECA-BARD uses a
 153 Bayesian framework to sample from the set of AR detector parameters that yield AR
 154 counts similar to the expert database of AR counts; this yields a set of “plausible” AR
 155 detectors from which we can assess quantitative uncertainty (O’Brien et al., 2020). We
 156 apply TECA-BARD to the ERA-20C data, and asses the plausible presence of an AR
 157 at a grid point where AR probability > 0.05 . While 0.05 is a low probability thresh-
 158 old, this indicates a non-zero probability of the existence of an AR in a given grid cell.
 159 Since TECA-BARD is inherently designed to detect ARs in mid-latitudes, it filters the
 160 IVT field near the tropics, resulting in AR probability that would have lower values in
 161 the presence of an AR in tropical latitudes than one in higher latitudes. We hypothe-
 162 size that AR probability > 0.05 represents a reasonable indication of the presence of an
 163 AR in lower latitudes. We test and show this in Sections 5 and 6.

164 2.2 Extreme Precipitation

165 We calculate the monthly 98th percentile precipitation rate value for ERA-20C and
 166 Livneh datasets at each grid cell. We define an *extreme precipitation event* for a given
 167 grid cell as the time when the precipitation is above the 98th percentile. We calculate
 168 the AR-associated extreme precipitation for each grid cell as the precipitation above the
 169 98th percentile when AR probability > 0.05 . Since the data record is sufficiently long
 170 (1900-2010 for ERA-20C and 1950-2013 for Livneh), we calculate all means and extreme
 171 precipitation quantiles monthly. The same holds for the atmospheric state composites
 172 described in Section 2.3.

173 2.3 Atmospheric State Composites

174 Following the methodology of (Neiman et al., 2008), we create composites of me-
 175 teorological variables to study the state of the atmosphere at the time of extreme pre-
 176 cipitation and AR events at two locations: Loc1 = 107.5W, 25N, and Loc2 = 105.0W, 21N
 177 (Figure 2, Loc1 denoted circle marker, Loc2 by the triangle). Loc1 is located close to the

maximum area of AR-associated precipitation and close to Culiacán Sinaloa, one of the most productive agricultural states of México. Loc2 is around the most southern region with AR-associated precipitation fraction ~ 0.5 , and in the state of Jalisco, another important agricultural producer in CWM. Both locations are close to the *Sierra Madre Occidental*, a mountain range that extends through Northwestern and Central-Western Mexico, as a part of the North American Cordillera, parallel to the coast. We hypothesize that if there is IVT normal to the *Sierra Madre* during the dry season, it could produce precipitation due to orographic lifting. The methodology to select the time steps to composite is as follows: we find the times when the AR probability is > 0.05 (ar), then we find all the times when the precipitation is above the 98th percentile (pr). We define then AR + extreme precipitation conditions as the times where both conditions ar and pr are met (ar_pr), times when there is ar but no pr (ar_noar), and times when there is pr but no ar (pr_noar). Finally, the long-term mean is the monthly climatology for 1900-2010 (ltm). We average in time for all the time in each composite and create monthly composites. Anomalies are calculated as the specific composite minus the long-term mean. Table 1 summarizes the different composite sampling.

Table 1. Atmospheric state composites. Composites are created monthly. The number of events at each location is the total number of events for all November-March months.

Atmospheric state composites

Conditions	Name	Anomaly	Events at Loc1	Events at Loc2
Climatology (long term mean)	ltm		134304	134304
AR	ar	$ar - ltm$	8886	4650
Extreme precipitation	pr	$pr - ltm$	2690	2688
AR/extreme precipitation	ar_pr	$ar_pr - ltm$	1549	1003
AR/no extreme precipitation	ar_noar	$ar_noar - ltm$	7337	3647
Extreme precipitation/no AR	pr_noar	$pr_noar - ltm$	1141	1685

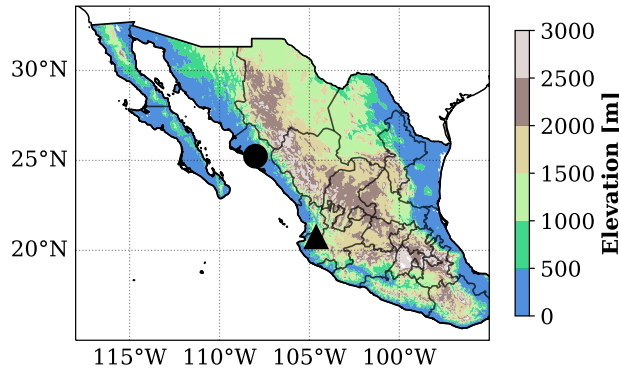


Figure 2. Orography of CWM. Loc1 and Loc2 are show in circle and triangle markers, respectively. The *Sierra Madre Occidental* is the mountain range that runs through Northwestern and Central-Western Mexico.

3 Results

In Section 3.1 we present the results of the AR-associated precipitation in CWM during the dry season (November-March) in the 1900-2010 period. We present the frac-

197 tional contribution of ARs to the precipitation, using ERA-20C data and the Livneh *et
198 al.* gridded dataset. Sections 5 through 6 focus on the meteorological state of the atmo-
199 sphere during extreme precipitation and AR events and the difference between differ-
200 ent composites. In the supplemental information, we include additional plots related to
201 the meteorological state of the atmosphere and differences between composites.

202 3.1 AR-associated extreme precipitation

203 Figure 3 shows how much of the CWM dry season precipitation is associated with
204 ARs. Figure 3(a) shows the fraction of ERA-20C total extreme precipitation amount as-
205 sociated with ARs, and (b) shows the same for Livneh precipitation. Figure 3(c) shows
206 the fraction of ERA-20C extreme precipitation frequency associated with ARs, and Fig-
207 ure 3(d) shows the same for Livneh precipitation. The results are highly condensed in
208 these figures, but they are clear and relevant: The influence of ARs in the dry season ex-
209 treme precipitation in CWM extends as far as \sim 17N. December has the highest AR-associated
210 precipitation, with \sim 75% of the frequency and amount 0.75 near Loc1, and between 50%
211 and 60% near Loc2. In general, we can say that in the Nov-March, more than half of the
212 extreme rainfall at Loc1 (more than 30% at Loc2) is associated with ARs, both in to-
213 tal amount and frequency.

214 We have shown the results based on two facts: the total amount of precipitation
215 (and frequency) higher than the monthly 98th percentile for November-March; and the
216 “plausible” presence of an AR in CWM given the `ar_probability` \geq 0.05. We hypoth-
217 esize that this precipitation is associated with low latitudes ARs and that `TECA_bard`
218 provides a good insight into the presence of ARs in CWM. This becomes clearer in Sec-
219 tion 5, where we present composites of the state of the atmosphere during `ar_probability` \geq 0.05
220 events at Loc1 and Loc2. For simplicity, in Section 4 and 5, we show the results for Jan-
221 uary. The supplemental information contains the results for the long-term mean and `ar_pr`
222 composites.

223 4 Long-term Mean

224 We briefly show the climatological state of the atmosphere (*ltm*) for January. The
225 long-term mean is calculated based using ERA-20C data. Figure 4(a) shows IWV be-
226 tween 10 and 15 kg m⁻² in CWM, with a maximum of 45 kg m⁻² near the ITCZ (be-
227 tween 5S and 5N). IVT is shown in Figure 4(b), with values between 0 and 100 kg m⁻¹s⁻¹
228 in CWM (IVT direction shown with vectors). We note a high IVT plume over the Pa-
229 cific storm track and higher IVT values between 5S and 5N associated with the ITCZ.
230 Mean sea level pressure depicts the North Pacific High with its maximum at 130W,30N,
231 shown in Figure 4(c). Geopotential height at 650 hPa, shown in Figure 4(d), has a large
232 gradient between 30N and 60N, associated with the jet stream over midlatitudes, with
233 very little or no spatial patterns over CWM and the central Pacific Ocean. The long-
234 term means for Nov-March are shown in the supplemental information (Figures S1 through
235 Figure S5). The general structure of the atmosphere is similar to 4(Low IVT and IWV
236 over CWM with the North Pacific High west of the coast of California and Baja Cali-
237 fornia), with slight differences in the locations of the ITCZ, storm track, North Pacific
238 High, etc.

239 5 Extreme Precipitation and AR Events Composite

240 In this section, we focus on the state of the atmosphere for the `ar_pr` composite (events
241 with extreme precipitation + AR probability \pm 0.05).

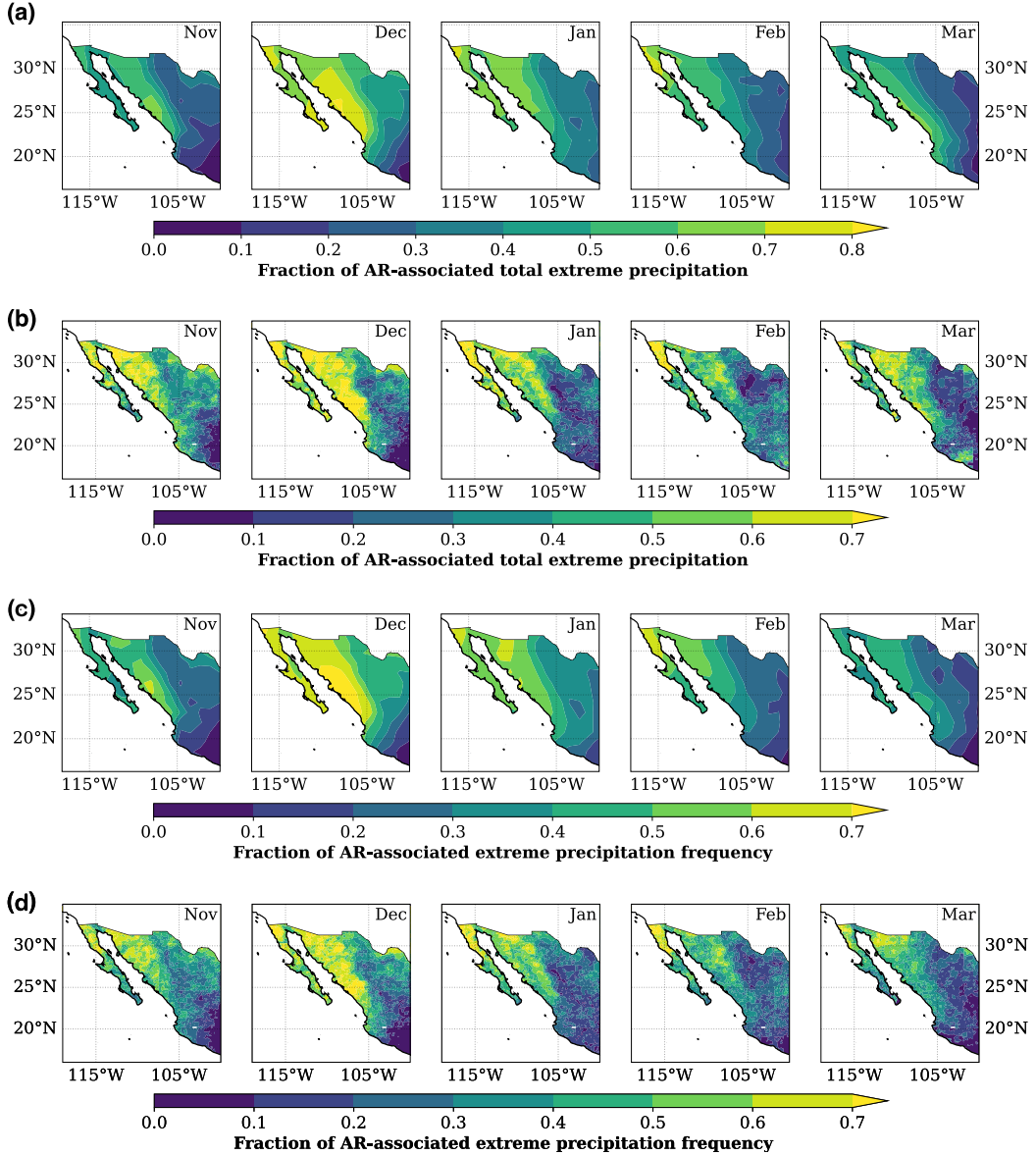


Figure 3. (a-b) Fraction of the total precipitation extreme precipitation (>98th percentile) associated with ARs. (a) ERA-20C 1900-2010. (b) Livneh 1950-2010. (c-d) Fraction of AR-associated to the total extreme (>98th) precipitation frequency. (c) ERA-20C 1900-2010. (d) Livneh 1950-2010

242

5.1 *ar-pr* composite at Loc1: Sinaloa, (107.5W, 25N)

243

Figure 5(a) shows IVT in colored contours and IWV in dashed white contours. We observe an elongated region of high IWV extending from the ITCZ into CWM, with values up to 30 kg m^{-2} at Loc1; as well as a ridge-like structure of high IVT (between 200 and $400 \text{ kg m}^{-1}\text{s}^{-1}$) centered at Loc1, similar to mid-latitude landfalling ARs (Neiman et al., 2008). Figure 5(b) shows IVT anomalies higher than $200 \text{ kg m}^{-1}\text{s}^{-1}$, and IWV anomalies up to 15 kg m^{-2} near Loc1. Mean sea level pressure (gray-filled contours in Figure 5(c)) shows the presence of the North Pacific High. Moreover, in 5(d), we observe a low in sea level pressure and geopotential height at 850 hPa anomalies centered near

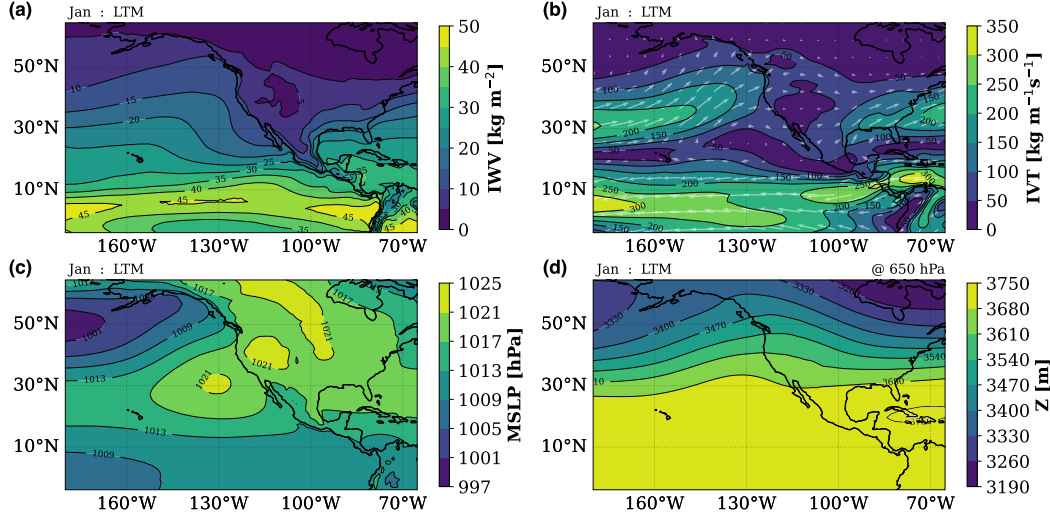


Figure 4. Long-term mean for 1900-2010 in December. (a) Integrated water vapor (IWV), (b) integrated vapor transport (IVT), (c) mean sea level pressure (MSLP), (d) geopotential height at 650 hPa. The vectors in panel (b) represent the direction of IVT.

115W,30N. This wave pattern is more noticeable in Figures 5(e) and (f) (geopotential height at 500 hPa). It is worth noticing that the low-pressure system at the surface is approximately aligned with the mid-troposphere low. This could imply that the wave producing this AR-pattern and anomalous dry season precipitation is barotropic. However, more analysis is needed to determine the nature and characteristics of these waves. Figures 5(g) and (h) show a mean negative vertical velocity (ascending) over the high IVT plume, ahead of the mid-tropospheric low (with anomalies $\sim 6 \text{ hPa s}^{-1}$). Vectors show the direction of IVT and its anomalies in Figures 5(g) and (h). IVT is normal to the mountain range and Loc1, with a weakening of the westward moisture transport near the Equator.

5.2 *ar-pr* composite at Loc2: Jalisco and Nayarit (105.0W,21N)

The *ar-pr* at Loc2 has a similar general structure to the Loc1, with slightly weaker IVT and higher IWV than the Loc1 composite. Figure 6(a) shows a high IVT ridge near Loc2 with a maximum value of $\sim 350 \text{ kg m}^{-1} \text{s}^{-1}$ and IWV $\sim 35 \text{ kg m}^{-2}$ near Loc2. The mean sea level pressure and geopotential show negative anomalies centered near 26N,110W, with lower magnitude than the Loc1 composite anomalies (Figures 6(c-f)). An upward 650 hPa wind velocity (and its anomaly) ahead of the tropospheric trough, with high IVT normal to the Sierra Madre at Loc2 (Figures 6(g) and (h)). The genesis and nature of the waves responsible for this weather pattern need to be further explored.

6 Difference between composites

This work focuses on the relationship between ARs and extreme precipitation during the dry season in CWM. In Section 5, we show the results for the *ar-pr* composite, *i.e.* when extreme precipitation and AR are present. This naturally raises the questions: *what about the other composites?*, *what is the difference between composites?*. For example, what is the difference between the climatology of events with extreme precipitation but no ARs detected (*pr-noar*)? What drives this anomalous rainfall? For simplicity, we focus the results in this section on composites over Loc1.

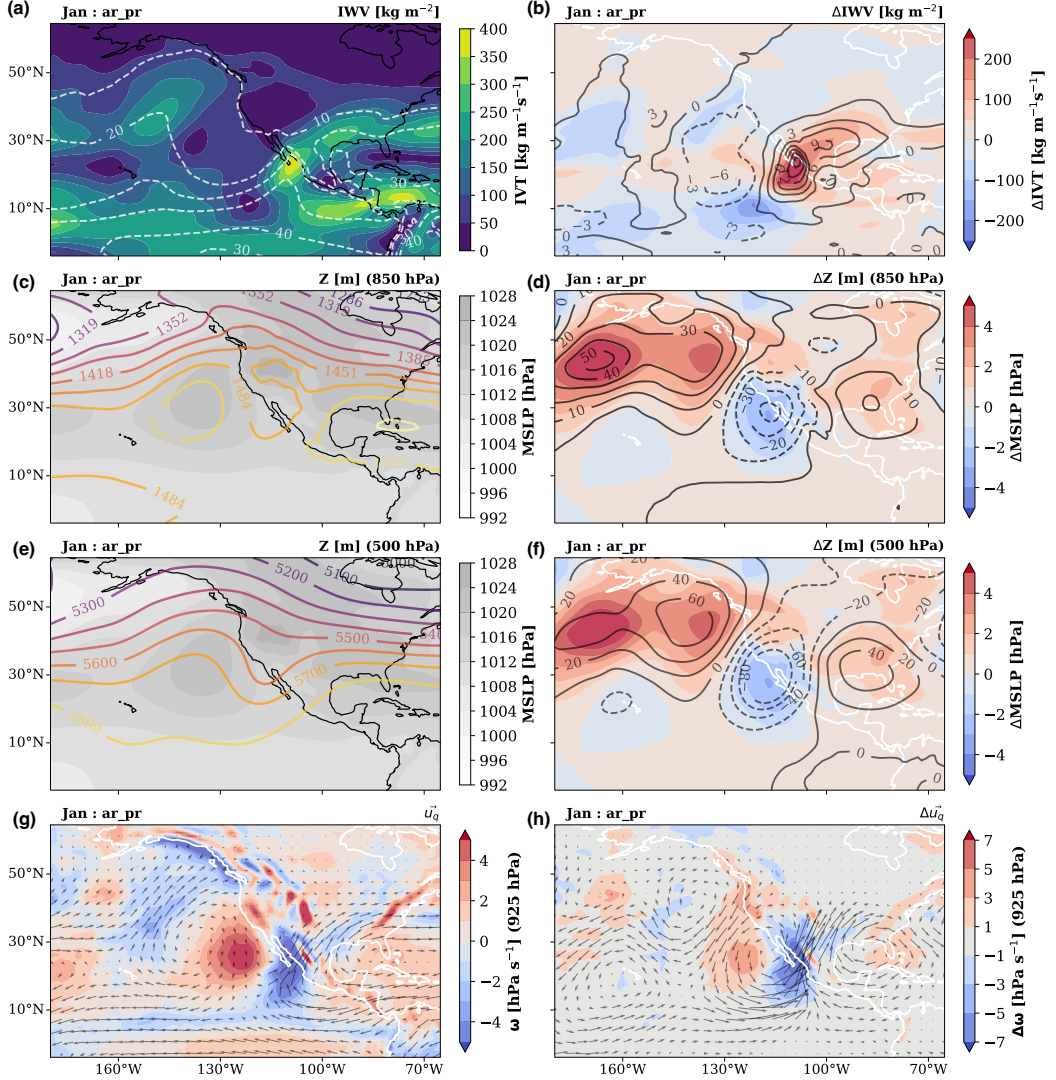


Figure 5. State of the atmosphere during AR landfalling and extreme precipitation at Loc1 in January. Contours variables are specified on the top-right of each plot. Left column: IWV, IVT, mean sea level pressure, geopotential height at 850 and 500 hPa, IVT direction (u_q), and ω at 650 hPa. Right column: anomalies with respect to the long-term mean for the same variables.

The IWV and IVT for January during extreme precipitation without detection of ARs (*pr_noar*) is shown in Figure 7(a,b). We observe that the general structure of IVT and IWV are similar to the *ar_pr* composite (surface pressure, geopotential height, and vertical velocity plots are shown in Figure S17). So, how different are they? In Figure 7(c,d), we observe little variation between the two composites for the pressure and 850 hPa geopotential height near CWM. The main differences in the pressure/geopotential fields are in the north part of the domain, where the wave pattern, present in both *ar_pr* and *pr_noar* is stronger for *ar_pr* (positive differences in Figure 7(d)). Nevertheless, the spatial patterns are similar between the two composites. Figure 7(c) shows moisture fields similar to *ar_pr*, although with weaker magnitudes in IVT and IWV for the *pr_noar* composite (Figure 7(c)), probably due to the weakening of the mid-troposphere wave pattern (Figure 7(d)).

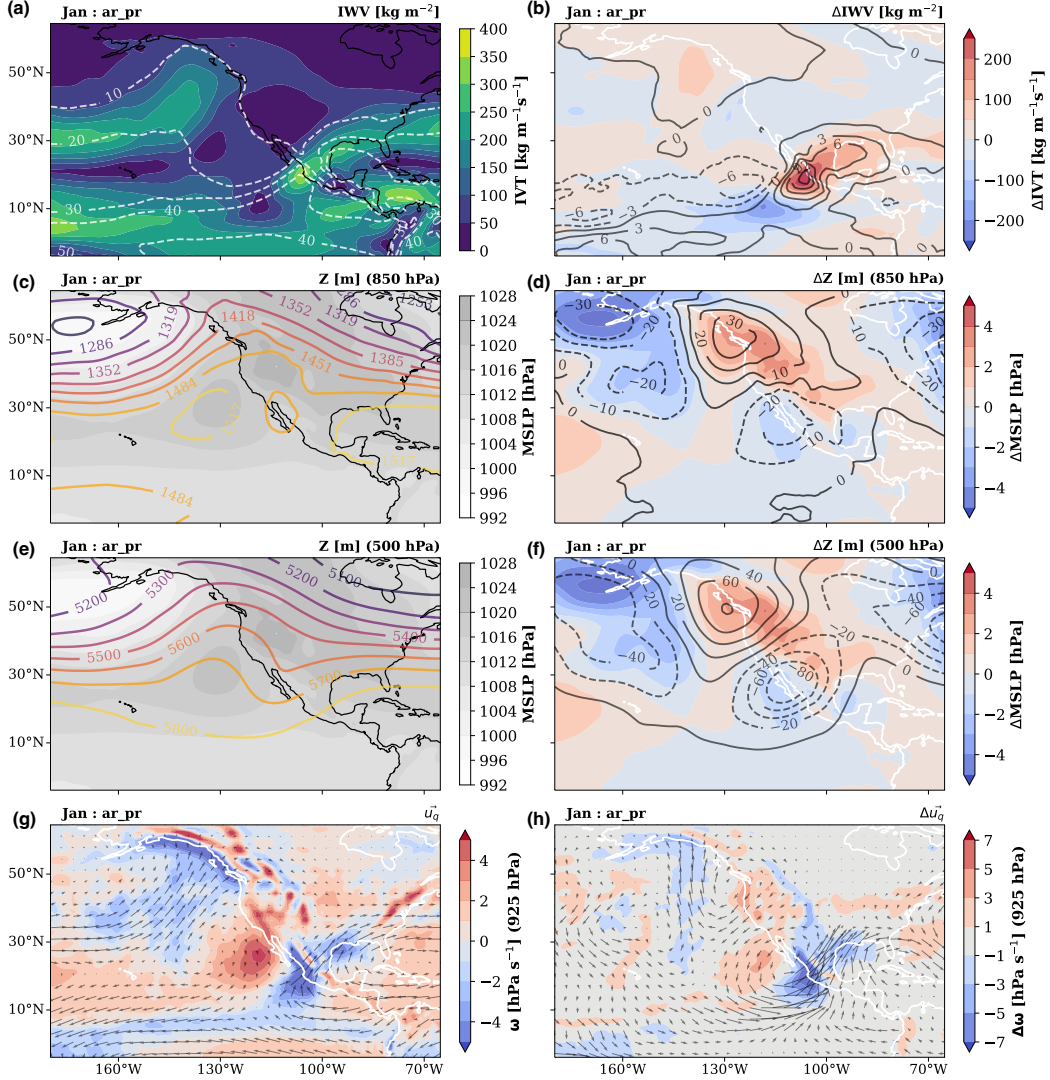


Figure 6. State of the atmosphere during AR landfalling and extreme precipitation at Loc2 in January. Contours variables are specified on the top-right of each plot. Left column: IWV, IVT, mean sea level pressure, geopotential height at 850 and 500 hPa, IVT direction (u_q), and ω at 650 hPa. Right column: anomalies with respect to the long-term mean for the same variables.

Figure 8(a,b) show the IWV and IVT for the *ar_nopr* composite in January, *i.e.* during AR detection without extreme precipitation present. We note a moisture transport into Loc1 (surface pressure, geopotential height, and vertical velocity plots are shown in Figure S16). In Figure 8, we notice differences between the *ar_nopr* and the *ar_pr* composites in surface pressure. The *ar_nopr* has a stronger pressure high in the northwest part of the domain but a weaker low high near CWM (Figure 8(d)). Moreover, a tilting in the geopotential height wave pattern (show in the supplemental information, Figure S16), and differences in its magnitude create a much weaker IVT magnitude and a difference in IVT direction at Loc1 (8(c)). This could be due to a stronger mid-troposphere wave associated with the jet stream meandering or the superposition of two or more waves. Again, the nature of the wave producing these weather patterns still needs to be explored and would make an exciting work by itself. Ultimately, the main consequence of these

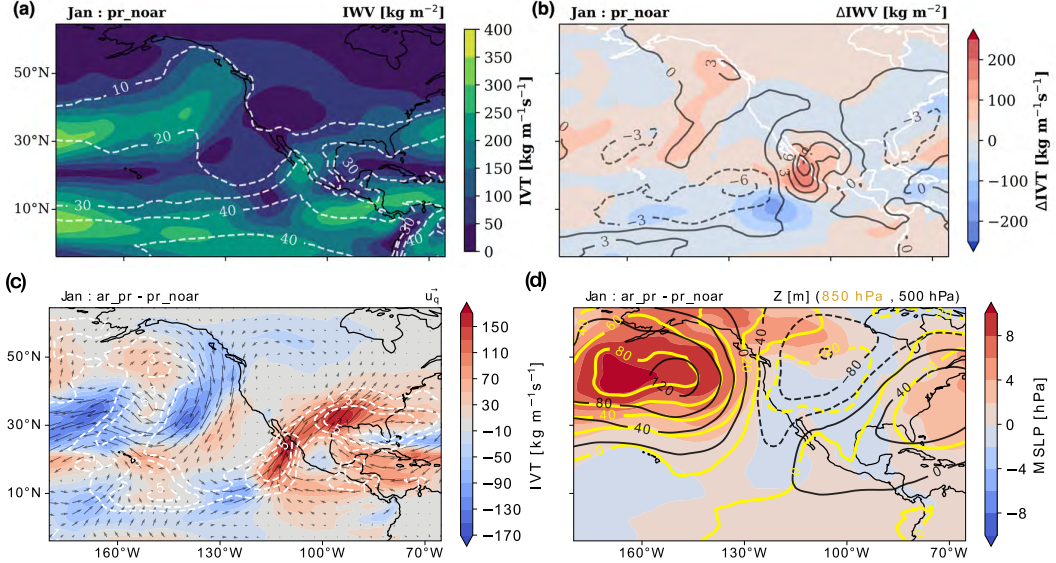


Figure 7. (a) IVT and IWV *pr_noar* composites for January and their anomalies (Loc1). (c and d) Differences in the atmospheric mean state between *ar_pr* and *pr_noar*. (c) IVT magnitude in filled contours, vectors represent IVT direction IVT, and white dashed contours denote changes in IWV. (d) Filled contours show mean sea level pressure differences, thick yellow contours show geopotential height at 850 hPa, and black contours geopotential height at 500 hPa.

302 wave differences is that they result in a much weaker IVT magnitude with a different di-
303 rection, both directly related to orographic precipitation.

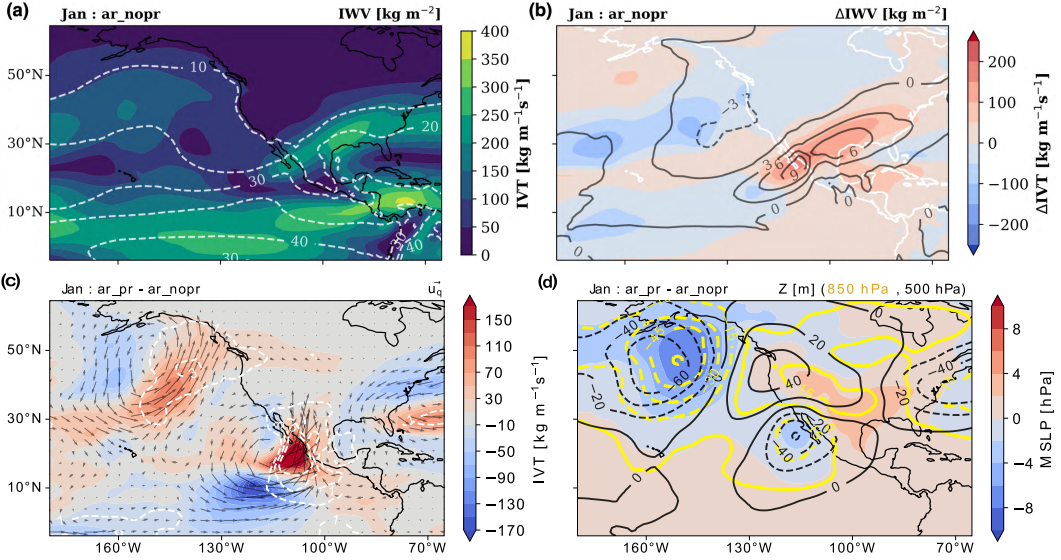


Figure 8. (a) IVT and IWV *pr_noar* composites for January and their anomalies (Loc1). (c and d) Differences in the atmospheric mean state between *ar_pr* and *ar_nopr*. (c) IVT magnitude in filled contours, vectors represent IVT direction IVT, and white dashed contours denote changes in IWV. (d) Filled contours show mean sea level pressure differences, thick yellow contours show geopotential height at 850 hPa, and black contours geopotential height at 500 hPa.

Figures 7(c,d) and 8(c,d) suggest that the different composites might be related to the same or similar weather events or different phases in the same weather event or wave. To explore this, we plot the occurrence time of the events for each composite, shown in the supplemental information's Figures S18-S25 (full 1900-2010 event composites time of occurrence at Loc1). There is, in fact, an overlap between composites; in some cases, precipitation events occur before or after ARs but around the same dates in general. This suggests that while we have acceptably identified AR events, an ARDT tuned for tropical latitudes could improve the AR detection in CWM, which could result in a greater correlation between ARs and dry season precipitation in CWM.

7 Discussion and Conclusions

There is a large amount of literature regarding the impacts of ARs in mid-latitudes and polar regions ((Gimeno et al., 2014; F. M. Ralph et al., 2017; Paltan et al., 2017; Rutz et al., 2019; Lora et al., 2020), and references therein) and AR changes with climate change ((Lavers et al., 2015; Payne et al., 2020; O'Brien et al., 2021), and references therein). Nonetheless, there is less research about ARs and their effects in lower latitudes (M. De Luna et al., 2020; M. I. De Luna, 2021). It is not until recently that tropical ARs have started to gather scientific interest. Moreover, since the summer precipitation (June-October) dominates the total precipitation of CWM, a significant part of the research has focused on the role of tropical storms, and tropical cyclones (Farfán & Fogel, 2007; Díaz et al., 2008; Agustín Breña-Naranjo et al., 2015; Dominguez, Christian and Magaña, Victor, 2018; Dominguez et al., 2020), and the role of the North American Monsoon (Adams & Comrie, 1997; Douglas & Englehart, 2007; Cavazos, Tereza and Arriaga-Ramírez, Sarahí, 2012). Furthermore, some studies associate the fluctuations and trends in precipitation in CWM with large-scale climate features like El Niño Southern Oscillation, Pacific Decadal Oscillation, and the Atlantic Multidecadal Oscillation (Magaña, Víctor and Pérez, Joel and Vázquez, Jorge and Pérez, José, 2003; Matías Méndez and Víctor Magaña, 2010; Curtis, 2007; Arriaga-Ramírez, Sarahí and Cavazos, Tereza, 2010). In particular, CWM appears to be a transition region between the Mediterranean rainfall regime in California and northern Baja California and the summer-dominated tropical rainfall regime and the North American Monsoon. This, together with the relatively developed AR research, has resulted in an overlook of the dry season (winter) precipitation and its association with tropical ARs.

Here, we present clear evidence of the relationship between CWM dry season precipitation and ARs. Our composites reflect a high degree of similarity with other compositing studios in higher latitudes (Neiman et al., 2008). Nevertheless, many aspects of these tropical ARs still need to be studied. Investigating the characteristics of the waves that create these anomalous IVT filaments and rainfall is key to understanding these weather patterns and their implications in the CWM dry season hydrological cycle. Moreover, ARs have been typically associated with mid-latitude baroclinic waves and extratropical cyclones (ETC). However, recently (Zhang et al., 2019) showed that nearly 20% of ARs are not nearby an ETC. Here we have presented evidence that aligned surface and mid-troposphere weaves are associated with tropical ARs in CWM, and could possibly denote a barotropic nature of these waves. There is no doubt that we still have a lot to learn and explore about ARs, particularly lower latitudes ARs. We still need to determine the genesis of these events. Are they more related to extratropical weather patterns like an amplification of mid-latitude waves? or maybe to tropical dynamics, energy balance, and responses to shifts in the ITCZ (Haffke & Magnusdottir, 2013; Choi et al., 2015; Lintner & Boos, 2019). In other words, *are these events, in fact, atmospheric rivers, or are they another weather phenomenon?*. We show clear evidence that there is a reasonable degree of similarity between winter ARs in CWM and typical mid-latitude ARs, so a more reasonable question may be *how similar or how different are tropical and mid-latitude ARs?*.

356 Although ARs in CWM do not dominate the total annual precipitation like on the
 357 US West Coast, they regulate extreme precipitation during the dry season. The water
 358 vapor in ARs frequently leads to heavy precipitation where they are forced upward by
 359 mountains (F. M. Ralph et al., 2018; Smith et al., 2009; F. Ralph et al., 2019). The pres-
 360 ence of the *Sierra Madre Occidental* in CWM provides creates an ideal mechanism for
 361 orographic rainfall during high IVT events in CWM. Therefore, it is relevant to quan-
 362 tify and understand these tropical ARs and their influence on the regional hydrological
 363 cycle of CWM. We recognize that this study (and future studies) could benefit from an
 364 ARDT tuned for tropical latitude, which brings back the question of how similar these
 365 ARs are to “traditional” mid-latitude ARs. The uncertainty in AR detection is key to
 366 answering this question. It has been discussed the possibility that there is more than one
 367 type of dynamical phenomenon that produces AR-like objects and that different defi-
 368 nitions for these processes could help in future studies (Inda-Díaz et al., 2021; O’Brien
 369 et al., 2021). This gains particular relevance for the study of future ARs in CWM, be-
 370 cause, in general, different “types” of AR-like phenomena (including CWM landfalling
 371 tropical ARs) could have different responses to climate change. There is some evidence
 372 of future AR frequency increases in lower latitudes (M. De Luna et al., 2020). Although
 373 the frequency increase magnitude is lower than for higher latitudes, there is no assur-
 374 ance on how the local hydrology will be impacted by changes in other AR quantities (in-
 375 tensity, size, orientation, geometry, among others).

376 In summary, we use data from the Atmospheric Reanalysis of the Twentieth Cen-
 377 tury ERA-20C and the TECA-BARD AR detector to demonstrate the relationship be-
 378 tween extreme precipitation and atmospheric rivers in central-western Mexico during the
 379 dry season (November-March) of 1900-2010. We find that more than 25% of extreme pre-
 380 cipitation amount and frequency are associated with ARs, with a maximum of 60%-80%
 381 during December and January near the coast of Sinaloa ($\sim 107.5^{\circ}\text{W}, \sim 25^{\circ}\text{N}$).

382 We calculate composites of the mean state of the atmosphere during AR and ex-
 383 treme precipitation events. We find that for the AR and precipitation composite (*ar-pr*),
 384 there is a positive anomaly in IWV and IVT. Horizontal vapor transport is normal to
 385 the coast and the mountain range of the Sierra Madre. Vertical velocity has upward anom-
 386 alies alongside the high IVT envelope. Besides, changes in horizontal moisture transport,
 387 sea level pressure, and geopotential height anomaly fields show a wave pattern associ-
 388 ated with the *ar-pr* composite. A weakening of the surface pressure high and the pres-
 389 ence of geopotential lows (above 850 hPa) suggest that the moisture transport occurs
 390 at a higher level than typical mid-latitude ARs.

391 Additionally, we examine the differences between composites. Our results suggest
 392 that the AR events without precipitation have a lower IVT magnitude. Furthermore,
 393 they show a tilted wave pattern in the geopotential height field with respect to the AR
 394 with precipitation composite. Taken together, this translates into lower horizontal va-
 395 por transport values with different orientations with respect to the mountain range, re-
 396 sulting in lower precipitation rates. Furthermore, we show that the main difference be-
 397 between the precipitation events with/and without ARs composite is IVT magnitude. Both
 398 composites have similar pressure and geopotential wave patterns near the coast of CWM.
 399 The pressure and low atmosphere geopotential main differences are located north of 30N.
 400 These results suggest that the precipitation without AR events, in fact, is related to the
 401 AR events. Both composites could be part of the same weather pattern that our ARDT
 402 failed to detect due to the lower IVT magnitude and its inherent design to filter out the
 403 tropics.

404 The nature and genesis of these anomalous IVT events and dry season precipita-
 405 tion –or apparent tropical ARs– still need to be determined, and we plan to explore them
 406 in future work. We recommend using more than one ARDT or one tuned explicitly for
 407 tropical latitudes, which could sharpen the correlation between ARs and CWM winter
 408 precipitation. This will allow investigating the response of CWM landfalling ARs to cli-

409 mate change, which could be critical for studying the region's hydroclimatology under
 410 future climate scenarios.

411 Acknowledgments

412 The authors thank the multiple reviewers and editors whose feedback and commen-
 413 tary greatly improved the quality and presentation of this manuscript.

414 This study was supported by the Director, Office of Science, Office of Biological
 415 and Environmental Research of the U.S. Department of Energy Regional and Global Mod-
 416 eling and Analysis (RGMA) and used resources of the National Energy Research Sci-
 417 entific Computing Center (NERSC), also supported by the Office of Science of the U.S. De-
 418 partment of Energy under Contract no. DE-AC02-05CH11231.

419 This project was supported by the Environmental Resilience Institute, funded by
 420 Indiana University's Prepared for Environmental Change Grand Challenge initiative.

421 CPC Global Unified Precipitation data provided by the NOAA/OAR/ESRL PSL,
 422 Boulder, Colorado, USA, from their Web site at <https://psl.noaa.gov/data/gridded/>
 423 [data.cpc.globalprecip.html](https://data.cpc.noaa.gov/globalprecip.html).

424 We would like to acknowledge the European Centre for Medium-Range Weather
 425 Forecasts and ERA-20C Project ([https://www.ecmwf.int/en/forecasts/datasets/
 426 reanalysis-datasets/era-20c](https://www.ecmwf.int/en/forecasts/datasets/reanalysis-datasets/era-20c)). ERA-20C was accessed through the Copernicus Cli-
 427 mate Change Service (C3S) Climate Data Store (CDS) - <https://apps.ecmwf.int/datasets/>
 428 [data/era20c-ofa/](https://data.ecmwf.int/era20c-ofa/).

429 We acknowledge Livneh, Ben & National Center for Atmospheric Research Staff
 430 (Eds). Last modified 12 Dec 2019. "The Climate Data Guide: Livneh gridded precip-
 431 itation and other meteorological variables for continental US, Mexico and southern Canada."
 432 Retrieved from [https://climatedataguide.ucar.edu/climate-data/
 433 livneh-gridded-precipitation-and-other-meteorological-variables-continental
 434 -
 435 us-mexico](https://climatedataguide.ucar.edu/climate-data/livneh-gridded-precipitation-and-other-meteorological-variables-continental-us-mexico).

436 This manuscript has been authored by authors at Lawrence Berkeley National Lab-
 437 oratory under Contract No. DE-AC02-05CH11231 with the U.S. Department of Energy.
 438 The U.S. Government retains, and the publisher, by accepting the article for publica-
 439 tion, acknowledges, that the U.S. Government retains a non-exclusive, paid-up, irrevo-
 440 cable, worldwide license to publish or reproduce the published form of this manuscript,
 441 or allow others to do so, for U.S. Government purposes

442 References

- 443 Magaña, Víctor and Pérez, Joel and Vázquez, Jorge and Pérez, José. (2003). Impact
 444 of el niño on precipitation in mexico. *Geofísica Internacional*. Retrieved from
 445 <https://www.redalyc.org/articulo.oa?id=56842304>
- 446 Adams, D. K., & Comrie, A. C. (1997). The north american monsoon. *Bulletin of the American Meteorological Society*, 78(10), 2197 - 2214. Retrieved from https://journals.ametsoc.org/view/journals/bams/78/10/1520-0477_1997_078_2197_tnam_2_0_co_2.xml doi: 10.1175/1520-0477(1997)078<2197:TNAM>2.0.CO;2
- 447 Agustín Breña-Naranjo, J., Pedrozo-Acuña, A., Pozos-Estrada, O., Jiménez-
 448 López, S. A., & López-López, M. R. (2015). The contribution of tropical
 449 cyclones to rainfall in mexico. *Physics and Chemistry of the Earth, Parts A/B/C*, 83-84, 111-122. Retrieved from <https://www.sciencedirect.com/science/article/pii/S1474706515000704> (Emerging science and appli-

- 456 cations with microwave remote sensing data) doi: <https://doi.org/10.1016/j.pce.2015.05.011>
- 457 Arriaga-Ramírez, Sarahí and Cavazos, Tereza. (2010). Regional trends of daily
458 precipitation indices in northwest mexico and southwest united states. *Journal
459 of Geophysical Research: Atmospheres*, 115(D14). Retrieved from <https://agupubs.onlinelibrary.wiley.com/doi/abs/10.1029/2009JD013248> doi:
460 <https://doi.org/10.1029/2009JD013248>
- 461 Breitburg, Denise; Grégoire, Marilaure and Isensee, Kirsten. (2018). *The ocean
462 is losing its breath: declining oxygen in the world's ocean and coastal waters;
463 summary for policy makers.* Retrieved from <https://unesdoc.unesco.org/ark:/48223/pf0000265196>
- 464 Cavazos, Tereza and Arriaga-Ramírez, Sarahí. (2012). Downscaled climate
465 change scenarios for baja california and the north american monsoon dur-
466 ing the twenty-first century. *Journal of Climate*, 25(17), 5904 - 5915. Retrieved
467 from <https://journals.ametsoc.org/view/journals/clim/25/17/jcli-d-11-00425.1.xml> doi: 10.1175/JCLI-D-11-00425.1
- 468 Chen, M., Shi, W., Xie, P., Silva, V. B. S., Kousky, V. E., Wayne Higgins, R., &
469 Janowiak, J. E. (2008). Assessing objective techniques for gauge-based
470 analyses of global daily precipitation. *Journal of Geophysical Research: At-
471 mospheres*, 113(D4). Retrieved from <https://agupubs.onlinelibrary.wiley.com/doi/abs/10.1029/2007JD009132> doi: <https://doi.org/10.1029/2007JD009132>
- 472 Choi, K.-Y., Vecchi, G. A., & Wittenberg, A. T. (2015). Nonlinear zonal
473 wind response to enso in the cmip5 models: Roles of the zonal and merid-
474 ional shift of the itcz/spcz and the simulated climatological precipita-
475 tion. *Journal of Climate*, 28(21), 8556 - 8573. Retrieved from <https://journals.ametsoc.org/view/journals/clim/28/21/jcli-d-15-0211.1.xml>
476 doi: 10.1175/JCLI-D-15-0211.1
- 477 Cruz López, M. (2011). Comparación del ciclo agrícola actual con el de hace unos
478 diez años en San Juan Jalpa municipio San Felipe Del Progreso Estado de
479 México: Evidencia de adaptación al cambio climático. *Ra Ximhai. Revista de
480 Sociedad, Cultura y Desarrollo Sustentable*, 7(1), 95–106.
- 481 Curtis, S. (2007, August). The atlantic multidecadal oscillation and extreme daily
482 precipitation over the US and mexico during the hurricane season. *Climate Dy-
483 namics*, 30(4), 343–351. Retrieved from <https://doi.org/10.1007/s00382-007-0295-0> doi: 10.1007/s00382-007-0295-0
- 484 De Luna, M., Waliser, D., Guan, B., Sengupta, A., Raymond, C., & Ye1, H. (2020).
485 *Tropical atmospheric rivers.* Paper presented at the Virtual Symposium by
486 the International Atmospheric Rivers Conference (IARC) Community, 5-9
487 October, 2020.
- 488 De Luna, M. I. (2021). Tropical atmospheric rivers. *Ph.D. dissertation, Califor-
489 nia State University, Los Angeles, ProQuest Dissertations Publishing.* Re-
490 trieved from <https://www.proquest.com/dissertations-theses/tropical-atmospheric-rivers/docview/2562506390/se-2?accountid=14505>
- 491 Dettinger, M. (2011). Climate change, atmospheric rivers, and floods in Cali-
492 fornia - a multimodel analysis of storm frequency and magnitude changes.
493 *Journal of the American Water Resources Association*, 47(3), 514–523. doi:
494 10.1111/j.1752-1688.2011.00546.x
- 495 Dettinger, M. D. (2013). Atmospheric Rivers as Drought Busters on the U.S. West
496 Coast. *Journal of Hydrometeorology*, 14(6), 1721–1732. doi: 10.1175/jhm-d-13-
497 -02.1
- 498 Dirmeyer, P. A., & Brubaker, K. L. (2007). Characterization of the Global Hy-
499 drologic Cycle from a Back-Trajectory Analysis of Atmospheric Water Vapor.
500 *Journal of Hydrometeorology*, 8(1), 20–37. doi: 10.1175/jhm557.1
- 501 Dominguez, C., Done, J. M., & Bruyère, C. L. (2020). Easterly wave con-

- tributions to seasonal rainfall over the tropical americas in observations
and a regional climate model. *Climate Dynamics*, 54(1), 191–209. Retrieved from <https://doi.org/10.1007/s00382-019-04996-7> doi: 10.1007/s00382-019-04996-7
- Dominguez, Christian and Magaña, Victor. (2018). The role of tropical cyclones in precipitation over the tropical and subtropical north america. *Frontiers in Earth Science*, 6. Retrieved from <https://www.frontiersin.org/article/10.3389/feart.2018.00019> doi: 10.3389/feart.2018.00019
- Domínguez-Hernández, G., Cepeda-Morales, J., Soto-Mardones, L., Rivera-Caicedo, J. P., Romero-Rodríguez, D. A., Inda-Díaz, E. A., ... Romero-Bañuelos, C. (2020, June). Semi-annual variations of chlorophyll concentration on the Eastern Tropical Pacific coast of Mexico. *Advances in Space Research*, 65(11), 2595–2607. Retrieved 2020-08-14, from <https://linkinghub.elsevier.com/retrieve/pii/S0273117720301113> doi: 10.1016/j.asr.2020.02.019
- Douglas, A. V., & Englehart, P. J. (2007). A climatological perspective of transient synoptic features during name 2004. *Journal of Climate*, 20(9), 1947 - 1954. Retrieved from <https://journals.ametsoc.org/view/journals/clim/20/9/jcli4095.1.xml> doi: 10.1175/JCLI4095.1
- Díaz, S., Salinas-Zavala, C., & Hernández-Vázquez, S. (2008, 04). Variability of rainfall from tropical cyclones in northwestern México and its relation to SOI and PDO. *Atmósfera*, 21, 213 - 223. Retrieved from http://www.scielo.org.mx/scielo.php?script=sci_arttext&pid=S0187-62362008000200006&nrm=iso
- Eldardiry, H., Mahmood, A., Chen, X., Hossain, F., Nijssen, B., & Lettenmaier, D. P. (2019). Atmospheric River-Induced Precipitation and Snowpack during the Western United States Cold Season. *Journal of Hydrometeorology*, 20(4), 613–630. doi: 10.1175/jhm-d-18-0228.1
- European Centre for Medium-Range Weather Forecasts. (2014). *Era-20c project (ecmwf atmospheric reanalysis of the 20th century)*. <https://doi.org/10.5065/D6VQ30QG>. Boulder CO: Research Data Archive at the National Center for Atmospheric Research, Computational and Information Systems Laboratory. ((Updated daily.) Accessed January 2022)
- Farfán, L. M., & Fogel, I. (2007, April). Influence of tropical cyclones on humidity patterns over southern baja california, mexico. *Monthly Weather Review*, 135(4), 1208–1224. Retrieved from <https://doi.org/10.1175/mwr3356.1> doi: 10.1175/mwr3356.1
- García Amaro de Miranda, E. (2003, 04). Distribución de la precipitación en la República Mexicana. *Investigaciones geográficas*, 67 - 76. Retrieved from http://www.scielo.org.mx/scielo.php?script=sci_arttext&pid=S0188-46112003000100009&nrm=iso
- Gershunov, A., Shulgina, T., Ralph, F. M., Lavers, D. A., & Rutz, J. J. (2017, aug.). Assessing the climate-scale variability of atmospheric rivers affecting western North America. *Geophysical Research Letters*, 44(15), 7900–7908. Retrieved from <http://doi.wiley.com/10.1002/2017GL074175> doi: 10.1002/2017GL074175
- Gimeno, L., Dominguez, F., Nieto, R., Trigo, R., Drumond, A., Reason, C. J., ... Marengo, J. (2016). Major Mechanisms of Atmospheric Moisture Transport and Their Role in Extreme Precipitation Events. *Annual Review of Environment and Resources*, 41(1), 117–141. doi: 10.1146/annurev-environ-110615-085558
- Gimeno, L., Nieto, R., Vázquez, M., & Lavers, D. A. (2014). Atmospheric rivers: a mini-review. *Frontiers in Earth Science*, 2(March), 1–6. doi: 10.3389/feart.2014.00002
- Goldenson, N., Leung, L. R., Bitz, C. M., & Blanchard-Wrigglesworth, E. (2018). Influence of atmospheric rivers on mountain snowpack in the western United States. *Journal of Climate*, 31(24), 9921–9940. doi:

- 566 10.1175/JCLI-D-18-0268.1
- 567 Guan, B., Molotch, N. P., Waliser, D. E., Fetzer, E. J., & Neiman, P. J. (2010). Extreme
568 snowfall events linked to atmospheric rivers and surface air temperature
569 via satellite measurements. *Geophysical Research Letters*, 37(20), 2–7. doi:
570 10.1029/2010GL044696
- 571 Haffke, C., & Magnusdottir, G. (2013). The south pacific convergence
572 zone in three decades of satellite images. *Journal of Geophysical Re-*
573 *search: Atmospheres*, 118(19), 10,839-10,849. Retrieved from <https://agupubs.onlinelibrary.wiley.com/doi/abs/10.1002/jgrd.50838> doi:
574 <https://doi.org/10.1002/jgrd.50838>
- 575 Huang, H., Patricola, C. M., Bercos-Hickey, E., Zhou, Y., Rhoades, A., Risser,
576 M. D., & Collins, W. D. (2021). Sources of subseasonal-to-seasonal predictabil-
577 ity of atmospheric rivers and precipitation in the western United States.
578 *Journal of Geophysical Research: Atmospheres*, 126, e2020JD034053. doi:
579 10.1029/2020JD034053
- 580 Inda-Díaz, H. A., O'Brien, T. A., Zhou, Y., & Collins, W. D. (2021). Con-
581 straining and characterizing the size of atmospheric rivers: A perspective
582 independent from the detection algorithm. *Journal of Geophysical Re-*
583 *search: Atmospheres*, 126(16), e2020JD033746. Retrieved from <https://agupubs.onlinelibrary.wiley.com/doi/abs/10.1029/2020JD033746>
584 (e2020JD033746 2020JD033746) doi: <https://doi.org/10.1029/2020JD033746>
- 585 Kim, J., Waliser, D. E., Neiman, P. J., Guan, B., Ryoo, J. M., & Wick, G. A.
586 (2013). Effects of atmospheric river landfalls on the cold season precipi-
587 tation in California. *Climate Dynamics*, 40(1-2), 465–474. doi: 10.1007/
588 s00382-012-1322-3
- 589 Lavers, D. A., Pappenberger, F., Richardson, D. S., & Zsoter, E. (2016). ECMWF
590 Extreme Forecast Index for water vapor transport: A forecast tool for atmo-
591 spheric rivers and extreme precipitation. *Geophysical Research Letters*, 43(22),
592 11,852–11,858. doi: 10.1002/2016GL071320
- 593 Lavers, D. A., Ralph, F. M., Waliser, D. E., Gershunov, A., & Dettinger, M. D.
594 (2015, jul). Climate change intensification of horizontal water vapor
595 transport in CMIP5. *Geophysical Research Letters*, 42(13), 5617–5625.
596 Retrieved from <http://doi.wiley.com/10.1002/2015GL064672> doi:
597 10.1002/2015GL064672
- 598 Lavers, D. A., & Villarini, G. (2013a). Atmospheric rivers and flooding over the cen-
599 tral United States. *Journal of Climate*, 26(20), 7829–7836. doi: 10.1175/JCLI
600 -D-13-00212.1
- 601 Lavers, D. A., & Villarini, G. (2013b). The nexus between atmospheric rivers and
602 extreme precipitation across Europe. *Geophysical Research Letters*, 40(12),
603 3259–3264. doi: 10.1002/grl.50636
- 604 Lavers, D. A., Waliser, D. E., Ralph, F. M., & Dettinger, M. D. (2016). Pre-
605 dictability of horizontal water vapor transport relative to precipitation: En-
606 hancing situational awareness for forecasting western U.S. extreme precipi-
607 tation and flooding. *Geophysical Research Letters*, 43(5), 2275–2282. doi:
608 10.1002/2016GL067765
- 609 Leung, L.-R., & Qian, Y. (2009). Atmospheric rivers induced heavy precipita-
610 tion and flooding in the western U.S. simulated by the WRF regional climate
611 model. *Geophysical Research Letters*, 36(3), 1–6. doi: 10.1029/2008GL036445
- 612 Lintner, B. R., & Boos, W. R. (2019). Using atmospheric energy transport to quan-
613 titatively constrain south pacific convergence zone shifts during enso. *Journal*
614 *of Climate*, 32(6), 1839 - 1855. Retrieved from <https://journals.ametsoc.org/view/journals/clim/32/6/jcli-d-18-0151.1.xml> doi: 10.1175/JCLI
615 -D-18-0151.1
- 616 Livneh, B., Bohn, T. J., Pierce, D. W., Munoz-Arriola, F., Nijssen, B., Vose, R.,
617 ... Brekke, L. (2015, August). A spatially comprehensive, hydrometeorolog-
- 618

- 621 ical data set for mexico, the u.s., and southern canada 1950–2013. *Scientific*
 622 *Data*, 2(1). Retrieved from <https://doi.org/10.1038/sdata.2015.42> doi:
 623 10.1038/sdata.2015.42
- 624 Livneh, Ben & National Center for Atmospheric Research Staff (Eds). (Last modified 12 Dec 2019). *ERA5: Fifth generation of ECMWF atmospheric reanalyses of the global climate*. <https://climatedataguide.ucar.edu/climate-data/livneh-gridded-precipitation-and-other-meteorological-variables-continental-us-mexico>.
- 625 Lora, J. M., Shields, C. A., & Rutz, J. J. (2020, oct). Consensus and Disagreement
 626 in Atmospheric River Detection: ARTMIP Global Catalogues. *Geophysical Research Letters*, 47(20), 1–10. Retrieved from <https://onlinelibrary.wiley.com/doi/10.1029/2020GL089302> doi: 10.1029/2020GL089302
- 627 Matías Méndez and Víctor Magaña. (2010). Regional aspects of prolonged meteorological droughts over mexico and central america. *Journal of Climate*,
 628 23(5), 1175 - 1188. Retrieved from <https://journals.ametsoc.org/view/journals/clim/23/5/2009jcli3080.1.xml> doi: 10.1175/2009JCLI3080.1
- 629 Neiman, P. J., Ralph, F. M., White, A. B., Kingsmill, D. E., & Persson, P. O.
 630 (2002). The statistical relationship between upslope flow and rainfall in
 631 California's coastal mountains: Observations during CALJET. *Monthly Weather Review*, 130(6), 1468–1492. doi: 10.1175/1520-0493(2002)130<1468:TSRBUF>2.0.CO;2
- 632 Neiman, P. J., Ralph, F. M., Wick, G. A., Lundquist, J. D., & Dettinger, M. D.
 633 (2008). Meteorological Characteristics and Overland Precipitation Impacts
 634 of Atmospheric Rivers Affecting the West Coast of North America Based on
 635 Eight Years of SSM/I Satellite Observations. *Journal of Hydrometeorology*,
 636 9(1), 22–47. doi: 10.1175/2007jhm855.1
- 637 Neiman, P. J., Ralph, M. F., Moore, B. J., Hughes, M., Mahoney, K. M., Cordeira,
 638 J. M., & Dettinger, M. D. (2013). The landfall and inland penetration of a
 639 flood-producing atmospheric river in Arizona. Part I: Observed synoptic-scale,
 640 orographic, and hydrometeorological characteristics. *Journal of Hydrometeorology*,
 641 14(2), 460–484. doi: 10.1175/JHM-D-12-0101.1
- 642 NOAA Physical Science Laboratory. (2008). *CPC global unified gauge-based analysis
 643 of daily precipitation*. Retrieved from [https://psl.noaa.gov/data/gridded/
 645 data.cpc.globalprecip.html](https://psl.noaa.gov/data/gridded/

 644 data.cpc.globalprecip.html)
- 646 O'Brien, T. A., Risser, M. D., Loring, B., Elbashandy, A. A., Krishnan, H., Johnson,
 647 J., ... Collins, W. D. (2020, dec). Detection of atmospheric rivers with inline
 648 uncertainty quantification: TECA-BARD v1.0.1. *Geoscientific Model Development*,
 649 13(12), 6131–6148. Retrieved from <https://www.geosci-model-dev-discuss.net/gmd-2020-55/#discussionhttps://gmd.copernicus.org/articles/13/6131/2020/> doi: 10.5194/gmd-13-6131-2020
- 650 O'Brien, T. A., Wehner, M. F., Payne, A. E., Shields, C. A., Rutz, J. J., Le-
 651 ung, L. R., ... Zhou, Y. (2021). Increases in future ar count and size:
 652 Overview of the artmip tier 2 cmip5/6 experiment. *Journal of Geophys-
 653 ical Research: Atmospheres*, e2021JD036013. Retrieved from <https://agupubs.onlinelibrary.wiley.com/doi/abs/10.1029/2021JD036013> doi:
 654 <https://doi.org/10.1029/2021JD036013>
- 655 Paltan, H., Waliser, D., Lim, W. H., Guan, B., Yamazaki, D., Pant, R., & Dad-
 656 son, S. (2017). Global Floods and Water Availability Driven by Atmo-
 657 spheric Rivers. *Geophysical Research Letters*, 44(20), 10,387–10,395. doi:
 658 10.1002/2017GL074882
- 659 Payne, A. E., Demory, M.-E., Leung, L. R., Ramos, A. M., Shields, C. A., Rutz,
 660 J. J., ... Ralph, F. M. (2020, mar). Responses and impacts of atmo-
 661 spheric rivers to climate change. *Nature Reviews Earth & Environment*,
 662 1(3), 143–157. Retrieved from <http://dx.doi.org/10.1038/s43017-020-0030-5> doi:
 663 <http://www.nature.com/articles/s43017-020-0030-5>

- 676 10.1038/s43017-020-0030-5
- 677 Poli, P., Hersbach, H., Dee, D. P., Berrisford, P., Simmons, A. J., Vitart, F., ...
 678 Fisher, M. (2016). Era-20c: An atmospheric reanalysis of the twentieth cen-
 679 tury. *Journal of Climate*, 29(11), 4083 - 4097. Retrieved from <https://journals.ametsoc.org/view/journals/clim/29/11/jcli-d-15-0556.1.xml>
 680 doi: 10.1175/JCLI-D-15-0556.1
- 681 Porter, J. R., & Semenov, M. A. (2005, November). Crop responses to cli-
 682 matic variation. *Philosophical Transactions of the Royal Society B: Bi-*
 683 *ological Sciences*, 360(1463), 2021–2035. Retrieved 2020-08-13, from
 684 <https://royalsocietypublishing.org/doi/10.1098/rstb.2005.1752>
 685 doi: 10.1098/rstb.2005.1752
- 686 Ralph, F., Rutz, J. J., Cordeira, J. M., Dettinger, M., Anderson, M., Reynolds, D.,
 687 ... Smallcomb, C. (2019, feb). A scale to characterize the strength and im-
 688 pacts of atmospheric rivers. *Bulletin of the American Meteorological Society*,
 689 100(2), 269–289. doi: 10.1175/BAMS-D-18-0023.1
- 690 Ralph, F. M., Coleman, T., Neiman, P. J., Zamora, R. J., & Dettinger, M. D.
 691 (2013, apr). Observed Impacts of Duration and Seasonality of Atmospheric-
 692 River Landfalls on Soil Moisture and Runoff in Coastal Northern California.
 693 *Journal of Hydrometeorology*, 14(2), 443–459. Retrieved from <https://journals.ametsoc.org/jhm/article/14/2/443/5819/Observed-Impacts-of-Duration-and-Seasonality-of> doi: 10.1175/JHM-D-12-076.1
- 694 Ralph, F. M., Dettinger, M., Lavers, D., Gorodetskaya, I. V., Martin, A., Viale, M.,
 695 ... Cordeira, J. (2017). Atmospheric rivers emerge as a global science and ap-
 696 plications focus. *Bulletin of the American Meteorological Society*, 98(9), 1969 -
 697 1973. Retrieved from <https://journals.ametsoc.org/view/journals/bams/98/9/bams-d-16-0262.1.xml> doi: 10.1175/BAMS-D-16-0262.1
- 698 Ralph, F. M., & Dettinger, M. D. (2011, aug). Storms, floods, and the science of
 699 atmospheric rivers. *Eos, Transactions American Geophysical Union*, 92(32),
 700 265–266. Retrieved from <https://onlinelibrary.wiley.com/doi/abs/10.1029/2011EO320001> doi: 10.1029/2011EO320001
- 701 Ralph, F. M., Dettinger, M. D., Cairns, M. M., Galarneau, T. J., & Eylander, J.
 702 (2018, apr). Defining “Atmospheric River”: How the Glossary of Meteorology
 703 Helped Resolve a Debate. *Bulletin of the American Meteorological Society*,
 704 99(4), 837–839. Retrieved from <http://journals.ametsoc.org/doi/10.1175/BAMS-D-17-0157.1> doi: 10.1175/BAMS-D-17-0157.1
- 705 Ralph, F. M., Neiman, P. J., Kiladis, G. N., Weickmann, K., & Reynolds, D. W.
 706 (2010, nov). A Multiscale Observational Case Study of a Pacific At-
 707 mospheric River Exhibiting Tropical–Extratropical Connections and a
 708 Mesoscale Frontal Wave. *Monthly Weather Review*, 139(4), 1169–1189. doi:
 709 10.1175/2010mwr3596.1
- 710 Ralph, F. M., Neiman, P. J., & Rotunno, R. (2005). Dropsonde observations in
 711 low-level jets over the northeastern Pacific Ocean from CALJET-1998 and
 712 PACJET-2001: Mean vertical-profile and atmospheric-river characteristics.
 713 *Monthly Weather Review*, 133(4), 889–910. doi: 10.1175/MWR2896.1
- 714 Ralph, F. M., Neiman, P. J., & Wick, G. A. (2004). Satellite and CALJET Air-
 715 craft Observations of Atmospheric Rivers over the Eastern North Pacific Ocean
 716 during the Winter of 1997/98. *Monthly Weather Review*, 132(7), 1721–1745.
 717 Retrieved from [http://journals.ametsoc.org/doi/abs/10.1175/1520-0493\(2004\)132<1721:SACAOO>2.0.CO;2](http://journals.ametsoc.org/doi/abs/10.1175/1520-0493(2004)132<1721:SACAOO>2.0.CO;2)
 718 doi: 10.1175/1520-0493(2004)132<1721:SACAOO>2.0.CO;2
- 719 Ralph, F. M., Neiman, P. J., Wick, G. A., Gutman, S. I., Dettinger, M. D., Cayan,
 720 D. R., & White, A. B. (2006). Flooding on California’s Russian River:
 721 Role of atmospheric rivers. *Geophysical Research Letters*, 33(13), 3–7. doi:
 722 10.1029/2006GL026689
- 723 Ralph, F. M., Rutz, J. J., Cordeira, J. M., Dettinger, M., Anderson, M., Reynolds,
 724 ...

- D., ... Smallcomb, C. (2019, feb). A Scale to Characterize the Strength and Impacts of Atmospheric Rivers. *Bulletin of the American Meteorological Society*, 100(2), 269–289. Retrieved from <https://journals.ametsoc.org/bams/article/100/2/269/69196/A-Scale-to-Characterize-the-Strength-and-Impacts> doi: 10.1175/BAMS-D-18-0023.1
- Romero-Rodríguez, D. A., Soto-Mardones, L. A., Cepeda-Morales, J., Rivera Caicedo, J. P., & Inda Díaz, E. A. (2020). Satellite-derived turbidity influence factors at small river mouths, tropical Pacific coast off México. *Advances in Space Research*. (Aceptado el 3 de agosto de 2020)
- Rutz, J. J., James Steenburgh, W., & Martin Ralph, F. (2014, feb). Climatological characteristics of atmospheric rivers and their inland penetration over the western united states. *Monthly Weather Review*, 142(2), 905–921. Retrieved from <https://journals.ametsoc.org/mwr/article/142/2/905/71947/Climatological-Characteristics-of-Atmospheric> doi: 10.1175/MWR-D-13-00168.1
- Rutz, J. J., Shields, C. A., Lora, J. M., Payne, A. E., Guan, B., Ullrich, P., ... Viale, M. (2019, dec). The Atmospheric River Tracking Method Inter-comparison Project (ARTMIP): Quantifying Uncertainties in Atmospheric River Climatology. *Journal of Geophysical Research: Atmospheres*, 124(24), 13777–13802. Retrieved from <https://onlinelibrary.wiley.com/doi/abs/10.1029/2019JD030936> doi: 10.1029/2019JD030936
- Simmons, A. J., & Burridge, D. M. (1981). An energy and angular-momentum conserving vertical finite-difference scheme and hybrid vertical coordinates. *Monthly Weather Review*, 109(4), 758 - 766. Retrieved from https://journals.ametsoc.org/view/journals/mwre/109/4/1520-0493_1981_109_0758_aeaamc_2_0_co_2.xml doi: 10.1175/1520-0493(1981)109(0758: AEAAMC)2.0.CO;2
- Smith, B. L., Yuter, S. E., Neiman, P. J., & Kingsmill, D. E. (2009). Water Vapor Fluxes and Orographic Precipitation over Northern California Associated with a Landfalling Atmospheric River. *Monthly Weather Review*, 138(1), 74–100. doi: 10.1175/2009mwr2939.1
- Viale, M., & Nuñez, M. N. (2011). Climatology of winter orographic precipitation over the subtropical central Andes and associated synoptic and regional characteristics. *Journal of Hydrometeorology*, 12(4), 481–507. doi: 10.1175/2010JHM1284.1
- Viale, M., Valenzuela, R., Garreaud, R. D., & Ralph, F. M. (2018). Impacts of Atmospheric Rivers on Precipitation in Southern South America. *Journal of Hydrometeorology*, 19(10), 1671–1687. doi: 10.1175/jhm-d-18-0006.1
- Viguera, B., Martínez-Rodríguez, M., Donatti, C., Harvey, C., & Alpízar, F. (2017). *Impactos del cambio climático en la agricultura de centroamérica, estrategias de mitigación y adaptación. materiales de fortalecimiento de capacidades técnicas del proyecto cascada (conservación internacional-catie)*. Conservación Internacional. Retrieved from https://www.conservation.org/docs/default-source/publication-pdfs/cascade_modulo-2-impactos-del-cambio-climatico-en-la-agricultura-de-centroamerica.pdf
- Waliser, D., & Guan, B. (2017). Extreme winds and precipitation during landfall of atmospheric rivers. *Nature Geoscience*, 10(3), 179–183. doi: 10.1038/ngeo2894
- Warner, M. D., Mass, C. F., & Salatheé, E. P. (2012). Wintertime extreme precipitation events along the Pacific Northwest Coast: Climatology and synoptic evolution. *Monthly Weather Review*, 140(7), 2021–2043. doi: 10.1175/MWR-D-11-00197.1
- Zhang, Z., Ralph, F. M., & Zheng, M. (2019). The Relationship Between Extratropical Cyclone Strength and Atmospheric River Intensity and Position. *Geophysical Research Letters*, 46(3), 1814–1823. doi: 10.1029/2018GL079071

- 786 Zhu, Y., & Newell, R. E. (1998). A Proposed Algorithm for Moisture Fluxes from
787 Atmospheric Rivers. *Monthly Weather Review*, 126(3), 725–735. doi: 10.1175/
788 1520-0493(1998)126<0725:apafmf>2.0.co;2